International Scholarly Research Network
ISRN Ceramics
Volume 2012, Article ID 943734, 6 pages
doi:10.5402/2012/943734

Research Article

Impedance and Electrical Modulus Study of Microwave-Sintered $SrBi_2Ta_2O_9$ Ceramic

V. Senthil,[1] T. Badapanda,[2] A. Chandra Bose,[3] and S. Panigrahi[1]

[1] *Department of Physics, National Institute of Technology, Orissa, Rourkela 769008, India*
[2] *Department of Physics, C. V. Raman College of Engineering, Orissa, Bhubaneswar 752054, India*
[3] *Department of Physics, National Institute of Technology, Tamilnadu, Tiruchirapalli 620015, India*

Correspondence should be addressed to V. Senthil, senthilv33@gmail.com

Received 6 December 2011; Accepted 9 January 2012

Academic Editors: Y. Laosiritaworn, A. Ravaglioli, and M. F. Zawrah

Bismuth layered structure $SrBi_2Ta_2O_9$ ceramic is prepared by the microwave sintering technique via solid state route at 1100°C for 30 mins. X-ray diffraction analysis is used to analyze the phase purity, which identifies the orthorhombic structure with $A2_1am$ space group. The fracture surface of the sintered pellet is visualized by scanning electron microscopy. Impedance spectroscopy is used to analyze the sample behavior as a function of frequency and temperature. Impedance and modulus study reveals the temperature-dependent non-Debye type relaxation phenomenon. The Nyquist plot shows a single arc representing the grain effect in the material, and the conductivity increases with increase in temperature. The Nyquist plot is fitted with an equivalent circuit, and the simulated parameters are well agreed with the calculated parameters. Arrhenius plot shows two different activation energies at below and above 300°C which identifies the phase transition of $SrBi_2Ta_2O_9$ ceramic. The fatigue property is explained by the basis of activation energies, which shows that SBT sintered by microwave technique is more fatigue resistant than conventional sintering.

1. Introduction

Ferroelectric random access memories (FeRAMs) show multiple advantages in memory devices like nonvolatile, less power consumption, high speed access, long communication distance, and long durability [1–3]. To meet commercial requirements for device lifetime, the ferroelectric materials in the FeRAM must have reliable polarization cycling characteristics. One of the most popular materials for this application is initially lead zirconate titanate (PZT) [1, 3]. However, PZT exhibits severe polarization fatigue during electric field cycling and also has hazardous effect. It has been suggested that fatigue in ferroelectric materials is a result of relatively high pinning energies for domain walls [4, 5].

Recently, bismuth layered structure ferroelectric materials have the keen interest in the memory applications due to fatigue free properties upto 10^{12} cycles [4, 5]. Bismuth layered structure ferroelectrics belong to a multilayer family of so-called Aurivillius phase with a general chemical formula $(Bi_2O_2)^{2+}(A_{m-1}B_mO_{3m+1})^{2-}$, where A represents larger size cations, B denotes smaller size cations, and $m = 2, 3, 4, \ldots$ refers to the number of BO_6 octahedra between neighboring Bi_2O_2 layers along the c-axis [6]. These BO_6 octahedra exhibit spontaneous polarization and $(Bi_2O_2)^{2+}$ layers act as the insulating paraelectric layers and mainly control the electrical response such as electrical conductivity, while the ferroelectricity arises mainly in the perovskite blocks [7, 8]. The primary reason for Aurivillius compounds not to have the fatigue problem is an oxygen vacancy in the $SrBi_2Ta_2O_9$ which is preferred in Bi_2O_2 layers, where the effect upon the polarization is negligible, and the effect is not within the $SrTaO_3$ octahedra that control ferroelectric switched polarization from Ta–O bonds [9, 10]. Moreover, the presence of unstable oxygen vacancies in the layers and their positioning in the lattice are supposed to compensate the space charges near the grain-electrode interfaces [11]. The electrical properties of the $SrBi_2Ta_2O_9$ systems are widely studied in bulk materials and thin films [12–15].

Microwave processing of ceramics gained much attention during the last decade. In the microwave heating

process, the heat is generated from the interior part of the material instead of the surface part, and hence there is an inverse heating profile. Due to the interaction of electromagnetic waves with the material, an energy conversion leads the heat to the material rather like energy transfer in conventional sintering. There is an almost 100% conversion of electromagnetic energy into heat, largely within the sample itself, unlike in conventional heating where there are significant thermal energy losses. Microwave heating has many advantages over conventional heating methods; they include rapid heating, enhanced densification rate, decreased sintering active energy, and improved microstructure. Microwave heating also has the potential for energy and cost savings when compared with conventional heating [16–18]. According to Xie et al. [18], the microwave sintering improves densification in short-time duration and the grain structures are much finer and more uniform, especially for high loss dielectric materials.

In this paper, we have tried the microwave-sintering technique as an alternative approach for conventional sintering of ceramics because of potential advantages such as rapid heating, penetrating radiation, more uniform microstructure, and hence higher density. Also, we explained the structural and electrical properties of bismuth layered ferroelectric $SrBi_2Ta_2O_9$ (SBT) ceramic. To the best of the author's knowledge, this is the first report on microwave sintered SBT ceramic.

2. Experimental Technique

Bismuth layered ferroelectric $SrBi_2Ta_2O_9$ (SBT) ceramic was prepared by solid state route via microwave sintering process. $Sr(NO_3)_2$ (99.0%) (Loba Chemie, Mumbai), Bi_2O_3 (99.9%), and Ta_2O_5 (99%) (Merck, Germany) were used as starting raw materials. Initially, stoichiometrically measured precursors were mixed and calcined at 1000°C for 30 minutes in the programmable microwave furnace. The calcined powder was mixed with 5% polyvinyl alcohol and pressed into disk under 60 MPa for 3 mins. Finally, disks were sintered in the same microwave furnace at 1100°C for 30 mins with a heating rate of 30°C/min by placing the pellets in the centre of a 4.4 kW, 2.45 GHz multimode microwave cavity. The sintered pellet was characterized by X-ray diffraction (XRD) (Powder X-Ray Diffractometer, Rigaku miniflex) for phase study, density measurement by Archimedes principles, morphological study of the fracture surface by using scanning electron microscope (SEM) (JEOL JSM6480, USA), elemental analysis by energy dispersive X-ray analysis (EDX), and electrical measurements by Solartron 1260A Gain/Phase analyzer. For electrical measurement, the pellet was polished and coated with silver paste for conducting electrodes. The electrical measurement data were collected from the computer interfaced Solartron 1260A Gain/Phase analyser between the frequency 100 Hz to 1 MHz. The measurements were performed over the temperature range from room temperature to 500°C at 1°C/min which was controlled by an interfaced Eurotherm temperature controller.

3. Results and Discussion

3.1. Phase Analysis and Morphology Study. Figure 1(a) represents the XRD pattern of sintered SBT pellet at 1100°C for 30 mins in a microwave furnace which shows well defined and prominent peaks corresponding to the standard data of JCPDS no. 49-0609. The diffraction peaks are allocated to the single phase layered structure ($m = 2$) with $A2_1am$ orthorhombic symmetry without any secondary phase. Lattice parameters and *hkl* indices have been analyzed by using *POWD* software. The lattice parameters are $a = 5.52091(10)$ Å, $b = 5.53945(09)$ Å, $c = 25.16583(31)$ Å and $V = 769.63$ Å^3. Orthorhombic distortion (b/a) value is 1.0034. Figure 1(b) shows the micrograph of the fractured structure of SBT ceramic sintered by the microwave technique at 1100°C for 30 mins. It can be seen that the clear grain growth and little amount of porosity are present with the 92% relative density.

3.2. Impedance and Modulus Spectroscopy. Figure 2(a) shows the imaginary part of impedance (Z'') versus frequency plotted at different temperatures from 225°C to 425°C. At lower temperatures (below 300°C), Z'' decreased monotonically, suggesting that relaxation is absent in the measured frequencies. This means that the relaxation species in the material are immobile species/electrons and orientation effects may be involved in the sample. Above 300°C, the nature of the Z'' start attains a maximum value at a particular frequency and the peak position varies with temperature which indicates the defects or the vacancies appearance at a high temperature [19]. The asymmetric variation in the broadness of the Z'' peaks suggested an electrical process with a spread of the relaxation time [19]. This variation shows considerable decrement in the magnitude of Z'' with a shift towards the higher side with temperature increases. The shifting of Z'' maximum towards a high frequency side explains the presence of temperature dependent on the relaxation phenomenon [20]. The decrement in the magnitude of Z'' with temperature indicates more conductivity due to the space charge in the material [21]. It also indicates the proportionality of resistance, that is, $Z'' = R_p/2$, where R_p is the calculated resistance [22]. At high frequency, the time for the space charges to relax and to recombine is less, so the space charge polarization is reduced with frequency increases and appears to merge at the high frequency for all the temperatures.

Figure 2(b) shows an imaginary part of electrical modulus with frequency for different temperatures. At the low frequency, the M'' value increases with frequency and reaches the maxima when it satisfies the relation $2\pi fRC = 1$, then it starts decreasing. The FWHM of these peaks shows more than 1.14 decades which confirm the non-Debye nature. The magnitude of M'' value decreases with temperature up to 300°C and then starts to increase, it indicates the relaxation process is different for below and above 300°C. The changes in the M'' magnitude with temperature indicate the changes in the capacitance value [22, 23], that is, $M'' = C_0/2C_p$, where C_p is the calculated capacitance and C_0 is the empty capacitance. This behavior

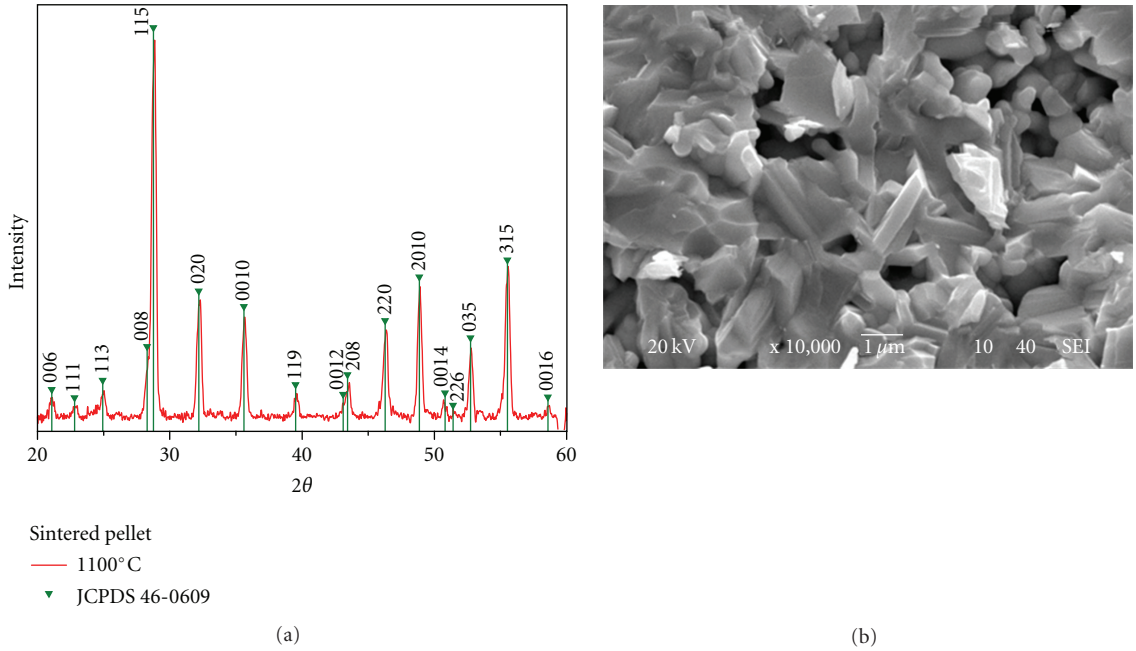

(a) (b)

Figure 1: (a) XRD pattern and (b) SEM of microwave-sintered SBT pellet at 1100°C for 30 mins.

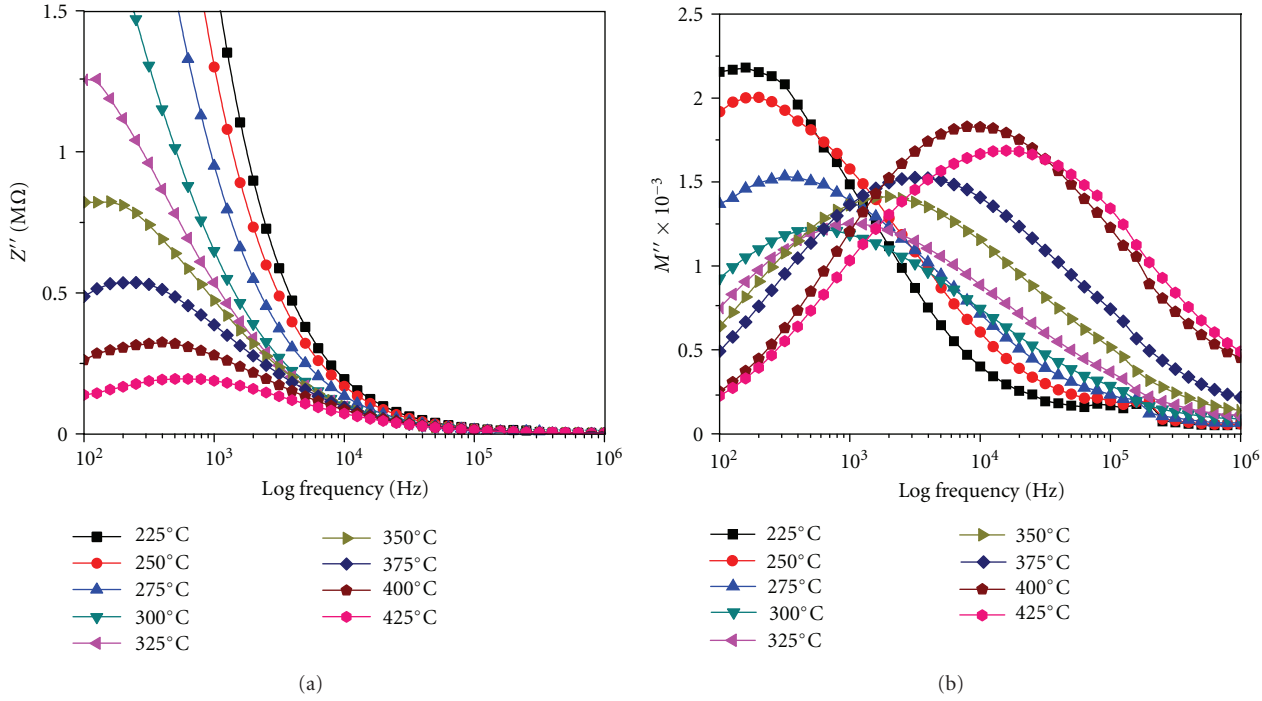

(a) (b)

Figure 2: (a) Imaginary part of Z'' and (b) M'' versus frequency for different temperatures of microwave-sintered SBT pellet.

suggests that the dielectric relaxation is thermally activated in which hopping mechanism of charge carriers dominates intrinsically [24].

3.3. Nyquist Plot. On the basis, an equivalent circuit is proposed with the parallel combination of a single R-CPE circuit as shown in Figure 3. Mathematical formalism is used to extract the parameters from the modeled equivalent circuit with the basis of complex impedance formula (Z^*). According to Debye model, the complex impedance is expressed as follows:

$$Z^* = \frac{R}{(1 + i\omega\tau)}, \quad (1)$$

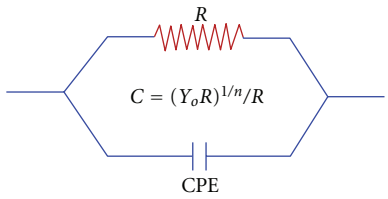

Figure 3: Proposed electrical equivalent circuit (R-CPE).

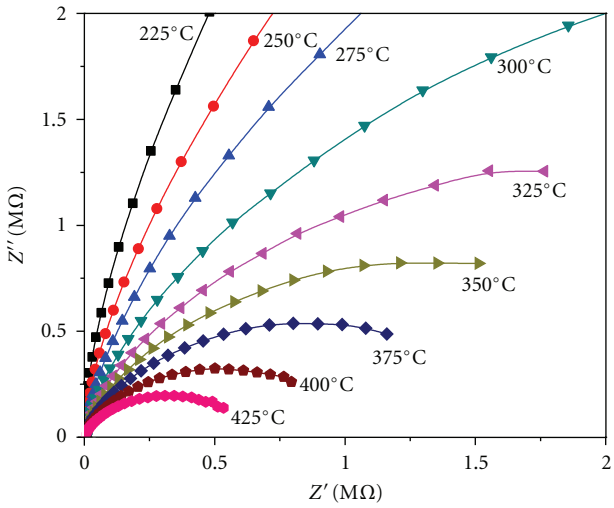

Figure 4: Complex impedance plot Z^* for different temperatures.

where ω is the angular frequency and τ is the relaxation time. It is well known that many dielectric relaxation processes can be described by the modified Debye model [25]:

$$Z^* = \frac{R}{(1 + i\omega\tau)^n}, \quad (2)$$

where $n = 1 - \phi$, $\theta = (1 - n)\pi/2$ and ϕ is the angle of deviation from the ideal semicircular arc. The simple Debye equation for the relaxation in the case for $\phi = 0$, that is, $n = 1$, shows pure capacitance and for $\phi = 1$, that is, $n = 0$, it shows complete resistance behavior. The plot for a resistor in parallel with a constant phase element is a semicircle depressed by an angle of $(1 - n)\pi/2$ with respect to Z'-axis. The CPE is not a pure electrical component. While several theories (surface roughness, "leaky" capacitor, nonuniform current distribution, etc.) have been proposed to account for the CPE, it is probably best to treat ϕ as an empirical constant with no real physical basis [25].

In Figure 4, the Nquist plot of Z^* of the samples sintered at 1100°C for 30 mins, which clearly shows the high insulating property (i.e., more resistance) and helps to enhance the dielectric property. The radius of the circle decreases with temperature confirming the negative temperature coefficient resistance (NTCR) behavior of the material, and the theoretical fitting is done by *ZView* software [25] with the modeled circuit (Figure 3). At the low temperature (below the 300°C), there is a linear response in Z'' and it indicates high insulating behavior in the

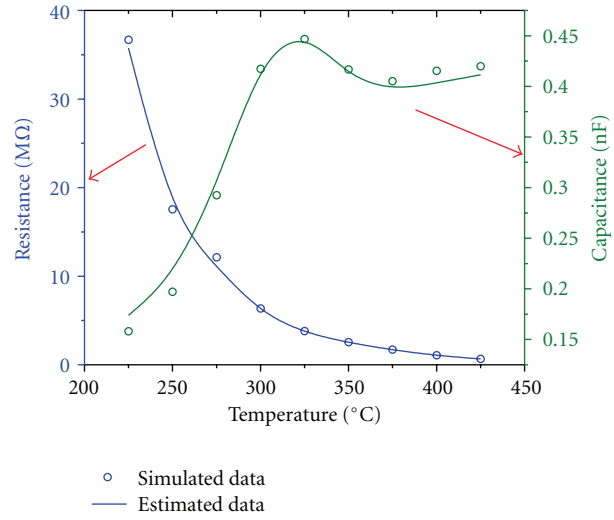

Figure 5: Graphical representation of the simulated (dot symbols) and estimated (solid line) parameters of resistance and capacitance.

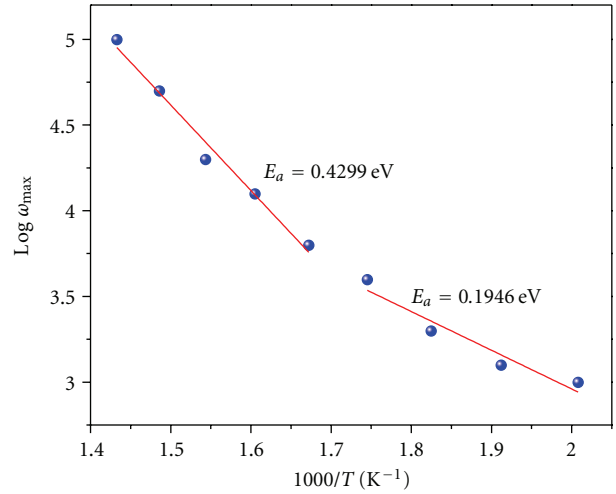

Figure 6: Arrhenius plot of relaxation frequency (from M''_{max}).

sample. As the temperature approaches 300°C, the linearity gradually changed to semicircular arc and it starts showing the relaxation behavior. The result of the simulated data with the corresponding equivalent circuit gives the value of resistance (R), constant phase element (Y_0), and exponent (n). The following expression is used to calculate the real capacitance (C) from the universal capacitance (CPE):

$$C = \frac{(Y_0 R)^{1/n}}{R}. \quad (3)$$

The simulated parameter of the equivalent circuit and the experimental values estimated are represented in Figure 5. The good agreement between the simulated and the estimated value confirms that the proposed model is perfectly fitted to the material property.

3.4. Activation Energy. Figure 6 shows the Arrhenius plot of temperature-dependent relaxation frequency from the

imaginary modulus plot. Activation energy will figure out the space charge transportations, which means, in the case of fewer oxygen vacancies, the space charge required more energies to migrate across the barrier because it restricts the movement and vice versa [26]. From the figure, it has been observed that there are two different activation energy slopes, that is, below and above 300°C, which shows the phase transition temperature of SBT ceramic. The activation energies of an earlier report by conventional method [12, 27] are much higher than the current report of pure SBT ceramic. So, lesser activation energy can transfer the space charge from the material to the cathode electrode easily and it can reduce the pinning of domain walls due to space charges trapped near the electrode [26]. Hence, it is concluded that the activation energy of the SBT sintered by microwave is less than that of the conventional sintered pellet which confirms the more fatigue resistance in the microwave sintered sample.

4. Conclusion

Bismuth layered $SrBi_2Ta_2O_9$ ceramic has been synthesized by Microwave sintering technique via solid state route at 1100°C for 30 mins. The XRD pattern shows the orthorhombic symmetry with the space group $A2_1am$, and the prominent peaks are well matched with the standard pattern. Grain growth and sintering quality are analyzed by scanning electron microscopy on fracture surface of the pellet. Impedance and modulus study shows that the single relaxation phenomenon with non-Debye type nature is confirmed by matching the estimated data with simulated data of the proposed circuit. Arrhenius plot shows two different activation energies at below and above 300°C which identifies the phase transition of SBT ceramic. The fatigue property is explained by the basis of activation energies, which concludes that more fatigue resistant in microwave sintered ceramic exists than in conventional sintering.

Acknowledgments

The authors would like to thank Prof T. P. Sinha, Bose Institute, Kolkatta for extending the facility of XRD and Prof P. Kumar, National Institute of Technology, Rourkela for extending the facility of the Microwave furnace.

References

[1] J. F. Scott, "The physics of ferroelectric ceramic thin films for memory applications," *Ferroelectric Review*, vol. 1, 1998.

[2] H. Sun, X. B. Chen, J. Zhu, J. H. He, Y. F. Qian, and H. Fang, "Notable enlargement of remnant polarization for fatigue-free $SrBi_4Ti_4O_{15}$ thin films by La-substitution," *Journal of Sol-Gel Science and Technology*, vol. 43, no. 1, pp. 125–129, 2007.

[3] G. C. C. da Costa, A. Z. Simões, A. Ries, C. R. Foschini, M. A. Zaghete, and J. A. Varela, "Phase formation and characterization of $BaBi_2Ta_2O_9$ obtained by mixed oxide procedure," *Materials Letters*, vol. 58, no. 11, pp. 1709–1714, 2004.

[4] C. A. Paz de Araujo, J. D. Cuchiaro, M. C. Scott, and L. D. McMillan, International Patent Application WO 93/12542, 1993.

[5] Y. Shimakawa, Y. Kubo, Y. Nakagawa et al., "Crystal structure and ferroelectric properties of $ABi_2Ta_2O_9$ (A=C*a*, Sr, and Ba)," *Physical Review B*, vol. 61, no. 10, pp. 6559–6564, 2000.

[6] G. N. Subbanna, T. N. G. Row, and C. N. R. Rao, "Structure and dielectric properties of recurrent intergrowth structures formed by the Aurivillius family of bismuth oxides of the formula $Bi_2A_{n-1}B_nO_{3n+3}$," *Journal of Solid State Chemistry*, vol. 86, no. 2, pp. 206–211, 1990.

[7] A. Rae, J. Thompson, R. Withers, and A. Willis, "Structure refinement of commensurately modulated bismuth titanate, $Bi_4Ti_3O_{12}$," *Acta Crystallographica B*, vol. 46, part 4, pp. 474–487, 1990.

[8] S. K. Kim, M. Miyayama, and H. Yanagida, "Electrical anisotropy and a plausible explanation for dielectric anomaly of $Bi_4Ti_3O_{12}$ single crystal," *Materials Research Bulletin*, vol. 31, no. 1, pp. 121–131, 1996.

[9] C. A. P. de Araujo, J. D. Cuchlaro, L. D. McMillan, M. C. Scott, and J. F. Scott, "Fatigue-free ferroelectric capacitors with platinum electrodes," *Nature*, vol. 374, no. 6523, pp. 627–629, 1995.

[10] J. F. Scott and M. Dawber, "Oxygen-vacancy ordering as a fatigue mechanism in perovskite ferroelectrics," *Applied Physics Letters*, vol. 76, no. 25, pp. 3801–3803, 2000.

[11] B. H. Park, S. J. Hyun, S. D. Bu et al., "Differences in nature of defects between $SrBi_2Ta_2O_9$ and $Bi_4Ti_3O_{12}$," *Applied Physics Letters*, vol. 74, no. 13, pp. 1907–1909, 1999.

[12] Y. Wu, M. J. Forbess, S. Seraji, S. J. Limmer, T. P. Chou, and G. Cao, "Impedance study of $SrBi_2Ta_2O_9$ and $SrBi_2(Ta_{0.9}V_{0.1})_2O_9$ ferroelectrics," *Materials Science and Engineering B*, vol. 86, no. 1, pp. 70–78, 2001.

[13] Y. Torii, K. Tato, A. Tsuzuki, H. J. Hwang, and S. K. Dey, "Preparation and dielectric properties of nonstoichiometric $SrBi_2Ta_2O_9$-based ceramics," *Journal of Materials Science Letters*, vol. 17, no. 10, pp. 827–828, 1998.

[14] N. Seong, C. Yang, W. Shin, and S. Yoon, "Oxide interfacial phases and the electrical properties of $SrBi_2Ta_2O_9$ thin films prepared by plasma-enhanced metalorganic chemical vapor deposition," *Applied Physics Letters*, vol. 72, no. 11, pp. 1374–1376, 1998.

[15] R. Dat, J. K. Lee, O. Auciello, and A. I. Kingon, "Pulsed laser ablation synthesis and characterization of layered Pt/$SrBi_2Ta_2O_9$/Pt ferroelectric capacitors with practically no polarization fatigue," *Applied Physics Letters*, vol. 67, pp. 572–574, 1995.

[16] D. K. Agrawal, "Microwave processing of ceramics," *Current Opinion in Solid State and Materials Science*, vol. 3, no. 5, pp. 480–485, 1998.

[17] Z. Xie, J. Yang, X. Huang, and Y. Huang, "Microwave processing and properties of ceramics with different dielectric loss," *Journal of the European Ceramic Society*, vol. 19, no. 3, pp. 381–387, 1999.

[18] Z. Xie, Z. Gui, L. Li, T. Su, and Y. Huang, "Microwave sintering of lead-based relaxor ferroelectric ceramics," *Materials Letters*, vol. 36, no. 1–4, pp. 191–194, 1998.

[19] P. Dhak, D. Dhak, M. Das, K. Pramanik, and P. Pramanik, "Impedance spectroscopy study of $LaMnO_3$ modified $BaTiO_3$ ceramics," *Materials Science and Engineering B*, vol. 164, no. 3, pp. 165–171, 2009.

[20] Y. Hosono, K. Harada, and Y. Yamashita, "Crystal growth and electrical properties of lead-free piezoelectric material $(Na_{1/2}Bi_{1/2})TiO_3$–$BaTiO_3$," *Japanese Journal of Applied Physics, Part 1*, vol. 40, no. 9 B, pp. 5722–5726, 2001.

[21] S. Mahajan, O. P. Thakur, D. K. Bhattacharya, and K. Sreenivas, "Ferroelectric relaxor behaviour and impedance

spectroscopy of Bi_2O_3-doped barium zirconium titanate ceramics," *Journal of Physics D*, vol. 42, no. 6, Article ID 065413, 2009.

[22] R. K. Dwivedi, D. Kumar, and O. Parkash, "Valence compensated perovskite oxide system $Ca_{1-x}La_xTi_{1-x}Cr_xO_3$. Part III: impedance spectroscopy," *Journal of Materials Science*, vol. 36, no. 15, pp. 3657–3665, 2001.

[23] U. Intatha, S. Eitssayeam, J. Wang, and T. Tunkasiri, "Impedance study of giant dielectric permittivity in $BaFe_{0.5}Nb_{0.5}O_3$ perovskite ceramic," *Current Applied Physics*, vol. 10, no. 1, pp. 21–25, 2010.

[24] P. Ganguly and A. K. Jha, "Impedance spectroscopy analysis of $Ba_5NdTi_3Nb_7O_{30}$ ferroelectric ceramic," *Physica B*, vol. 405, no. 15, pp. 3154–3158, 2010.

[25] "Basics of Electrochemical Impedance Spectroscopy," *Application note*, Gamry Instruments, 734 Louis Drive Warminster, PA 18974 USA.

[26] M. M. Kumar and Z. G. Ye, "Dielectric and electric properties of donor- and acceptor-doped ferroelectric $SrBi_2Ta_2O_9$," *Journal of Applied Physics*, vol. 90, no. 2, pp. 934–941, 2001.

[27] B. Sih, A. Jung, and Z. G. Ye, "Effects of silver doping on ferroelectric $SrBi_2Ta_2O_9$," *Journal of Applied Physics*, vol. 92, no. 7, pp. 3928–3935, 2002.